Acoustic matching of a traveling-wave thermoacoustic electric generator

Kai Wang[a,b,c], Jie Zhang[a,b], Ning Zhang[a,b], Daming Sun[a,b *], Kai Luo[a,b], Jiang Zou[a,b], Limin Qiu[a,b]

[a] *Institute of Refrigeration and Cryogenics, Zhejiang University, Hangzhou 310027, PR China*

[b] *Key Laboratory of Refrigeration and Cryogenic Technology of Zhejiang University*

[c] *Energy Research Institute @ NTU, Nanyang Technological University, Singapore 637141*

Abstract

Acoustic impedance matching is critical to the overall performances of a traveling-wave thermoacoustic electric generator. This paper presents an effective approach for matching the acoustic impedances of the thermoacoustic engine and the linear alternators for maximizing the output electric power and thermal-to-electric efficiency. The acoustic impedance characteristics of the engine and the linear alternators are analyzed separately, and the methods for modulating the acoustic impedances are investigated numerically. Specially, two different coupling locations including one at the resonator and the other one at the loop of the thermoacoustic engine are compared. It is found that the imaginary part of the load acoustic impedance should be near zero for a good output performance of the engine at either coupling location. The real part of the optimal acoustic impedance for the coupling location at the resonator is smaller than that for the one at the loop. The acoustic impedance of the linear alternator can be simply and effectively adjusted to the expected range by tuning the operating frequency, load resistance and the electric capacitance. Both the experiments and numerical simulations show that a better matched condition can be achieved when they are coupled at the location at the resonator. Maximum output electric power of 750.4 W and the highest thermal-to-electric efficiency of 0.163 have been achieved. When they are coupled at the loop, the maximum electric power and the thermal-to-electric efficiency become 506.4 W and 0.146 due to the lower quality of the acoustic matching. The acoustic matching approach presented in the paper would be helpful for guiding the designs of thermoacoustic/alternator and compressor/cryocooler systems.

Keywords: thermoacoustic; linear alternator; acoustic impedance; impedance match

[*] Corresponding author. Tel/Fax: +86-571-87952769 (Daming Sun)
E-mail address: wangkai7089@gmail.com (Kai Wang), sundaming@zju.edu.cn (Daming Sun)

1. Introduction

Traveling-wave thermoacoustic electric generator is capable of converting thermal energy into electric power with high reliability and efficiency with very simple structures. It is typically composed of a traveling-wave thermoacoustic engine [1-7] or several traveling-wave thermoacoustic conversion units [8, 9] that consist of a hot heat exchanger, a regenerator and a cold heat exchanger, and several linear alternators. The externally added thermal energy is first converted into acoustic energy by the thermoacoustic engine, and then into electric power by the linear alternators.

In recent ten years, many research groups have been devoted into the developments of the thermoacoustic electric generation system, and great progress has been made. The earliest thermoacoustic electric generator was built by Backhaus et al. [10] in 2004, which achieved an electric power of tens of watts. The long resonator in a traditional traveling-wave thermoacoustic engine is firstly completely replaced by the linear alternators in the system. Sunpower, Inc. later developed a similar traveling-wave thermoacoustic electric generator with an output power of about 50 W [11]. Wang et al. experimentally optimized the shapes of the phase adjusting components at the coupling port of a small traveling-wave thermoacoustic electric generator and achieved about 73 W electric power [12]. Luo et al. [9, 13-15] have conducted a series of research work on traveling-wave thermoacoustic electric generators. They proposed a double-acting thermoacoustic electric generator removing the long gas resonator, which is composed of three sets of thermoacoustic conversion units and three linear alternators arranged in a loop [15]. The designed 3 kW-scale system achieved the maximum electric power of 1.57 kW with an efficiency of 16.8%. Later, a three-stage resonant thermoacoustic electric generator capable of generating about 5 kW electric power was developed [9]. Sun et al. [16, 17] were also engaged into the developments of traveling-wave thermoacoustic electric generators recently. The effects of the mechanical and electric resonances on the performances of a traveling-wave thermoacoustic electric generator with a resonator were investigated [16]. An electric power of 345.3 W and a thermal-to-electric efficiency of 12.33% were achieved. After further optimizations, the system was able to achieve 473.6 W electric power and 14.5% thermal-to-electric efficiency [17]. Several other research groups adopted low-cost loudspeakers as the electric convertors in traveling-wave thermoacoustic electric generators [18-21]. The achieved electric powers ranged from several watts to about 200 W and the thermal-to-electric efficiencies were typically less than 5%.

In a traveling-wave thermoacoustic engine, the linear alternators act as the acoustic load to the thermoacoustic engine. The acoustic impedance of the linear alternators has great effects on the performances of the engine. Besides, the required acoustic impedance for coupling the thermoacoustic engine also affects the acoustic-to-electric conversion of the linear alternators. Therefore, the match of the acoustic impedances between the thermoacoustic engine and the linear alternator is critical to the overall performance. In some cases, the system is even not able to work if they don’t match.

Swift [22] pointed out that the best position for placing an acoustoelectric transducer in a standing-wave resonator depends on the acoustic impedance of the transducer itself. High-impedance transducer should be placed at a point of high acoustic impedances, and a low-impedance transducer is best located at a point of low acoustic impedances. This is one of the earliest statements about the impedance match in a thermoacoustic system. Several researchers [23-27] used the equivalent circuit method to obtain the equivalent acoustic impedances of the acoustoelectric transducers, and then coupled it with standing-wave thermoacoustic systems. The effects of the frequency on the efficiencies of the transducers were extensively studied. However, the effects of the acoustic impedance on the performance of the thermoacoustic system and whether the systems were acoustically well matched have not been studied by the above work. Dai et al. [28] studied the impedance match for Stirling type cryocoolers. The study mainly focused on the requirements of the acoustic impedance for maximizing the efficiency and output acoustic power of the linear compressors, while the characteristics of the cryocooler part were not considered. Hatori et al. [29] reported an experimental method to determine the acoustic impedances of a traveling-wave thermoacoustic loop and its acoustic load by using an acoustic driver. Sun et al. [5] studied the output characteristics of a traveling-wave thermoacoustic engine, and showed that the output position have great effects on the output performances. It was demonstrated that the double output method helped to improve the output performances. Zhang et al. [30] studied the output characteristics of a traveling-wave thermoacoustic engine numerically and experimentally. RC-type and RL-type acoustic loads driven by the engine were studied and compared. It was shown that the acoustic impedance is critical and unique for a good output performance. The work is helpful for designing an appropriate acoustic load to couple with the engine. In the studies about the small thermoacoustic electric generator, Backhaus et al. [10] pointed out that the moving mass of the linear alternators should be in a resonance state under the combined actions of the forces from the gas spring, the flexure bearing and the electromagnetism effect. The details about the designs and impedance match were not presented. In the work about the kW-class thermoacoustic electric generator of Ref. [14], the system was not operated at its optimal acoustic impedance when pure helium is used as the working gas due to the mismatch of the working frequency. Argon-helium mixed gas was used to decrease the frequency so as to have a better impedance match. In all, there are few detailed and comprehensive studies about the impedance match between the thermoacoustic engine and the alternators in thermoacoustic electric generation systems. Particularly, the effects of the coupling positions of the linear alternators on the performance of the thermoacoustic electric generation systems have never been studied. How to match the system effectively by modulating the acoustic impedances of the engine and the linear alternators to achieve the best performance still remains a question.

In this paper, the acoustic impedance match in a traveling-wave thermoacoustic electric generator is studied numerically and experimentally. The general procedure to match the thermoacoustic engine and the linear alternators to reach an acoustically well matched working condition is presented. The acoustic impedance characteristics of the thermoacoustic engine and the

linear alternators are then calculated and analyzed individually. Two different locations for coupling the linear alternators are investigated and compared. Several effective measures are used to match the acoustic impedances. Experiments are finally conducted to verify the numerical analysis and demonstrate the acoustically well matched working conditions.

2. Procedure of acoustic impedance match

Acoustic impedance denotes the ratio of pressure to volume flow rate in acoustic systems, such as thermoacoustic engines, pulse tube refrigerators, etc. Acoustic impedance Z_a is defined by,

$$Z_a = \mathrm{Re}[Z_a] + j \cdot \mathrm{Im}[Z_a] = \frac{p_1}{U_1} = \frac{|p_1|}{|U_1|}\cos\theta_{p-U} + j \cdot \frac{|p_1|}{|U_1|}\sin\theta_{p-U} \tag{1}$$

where, p_1 and U_1 denote the complex pressure amplitude and volume flow rate amplitude, respectively; θ_{p-U} is the phase difference between the pressure and volume flow rate.

A traveling-wave thermoacoustic electric generator is generally composed of a traveling-wave thermoacoustic engine and several linear alternators. When the acoustic impedance is matched in a thermoacoustic electric generator, it means that the thermoacoustic engine and the linear alternators can both work at or near their optimal working conditions simultaneously when they are connected. The coupled system is able to achieve the maximum electric power output and the highest thermal-to-electric efficiency at its full potential. In order to achieve the matching condition stated above, three aspects of matching should be considered. Firstly, the frequencies of the engine and the alternators should be matched so that the coupled system is harmonically operated. Secondly, the required acoustic impedances to reach the optimal performances of the engine and the alternators should be matched. In other words, they can be both operated at the optimal states simultaneously at a certain acoustic impedance and frequency. Thirdly, the output acoustic power of the engine and the acoustic power that can be extracted by the alternators should be matched.

In previous studies on thermoacoustic systems, it was a regular approach to first build a complete model of the whole system, and then investigate the effects of different parameters on the system performances so as to find the direction for optimization. It is worth noting that the thermoacoustic engine and the linear alternators not only work synergistically as a coupled system, but also work independently in a thermoacoustic electric generator. If the aforementioned approach is used in such a strongly coupled system, the critical information about the optimal working conditions that the engine and the alternators require may be covered. It is difficult to know whether the sub-systems have reached their optimal working conditions if only the whole model is investigated. Besides, due to so many adjustable parameters in the whole system, it is also a challenge to find the clear direction for the optimization and realize the acoustic match between the engine and the alternators.

In electrics, an effective way of realizing the electric impedance match in a power circuit is to introduce the concepts of input impedance of the electric load and the output impedance of the

electric source, and design the load and electric source separately. When the input and output impedances are adjusted to be the same, the electric load and the source can be matched to form a more complex electric circuit. Inspired by the idea, we propose to realize the acoustic impedance match of the thermoacoustic electric generator in the procedure illustrated in Figure 1. The characteristics of the required acoustic impedances for the operations of the engine and alternators are first analyzed independently. According to the requirements of the acoustic impedances, their acoustic impedances are then adjusted to be the same when they can operate at or near their optimal states simultaneously. Finally, the engine and the alternators are coupled at the modulated acoustic impedance.

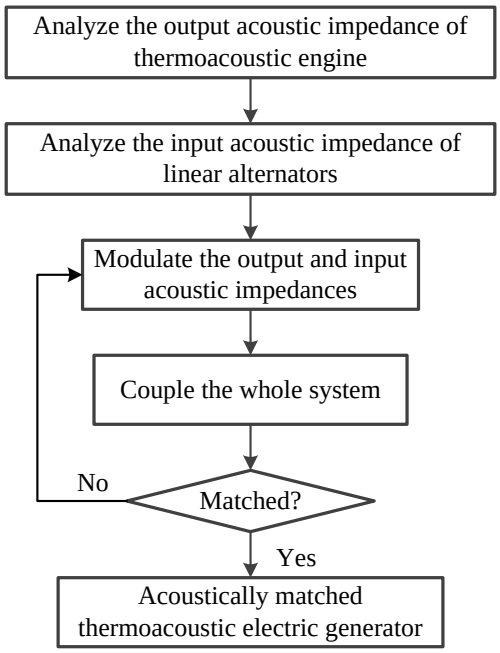


Figure 1. Procedure of impedance matching of thermoacoustic electric generator.

3. Experimental Setup

Figure 2 illustrates the schematic of the traveling-wave thermoacoustic engine [17]. It mainly consists of a regenerator, several heat exchangers, a feedback loop and a gas resonator. The regenerator (REG) is the key component where thermoacoustic energy conversion happens, and is filled with stainless steel screens with a mesh number of 120. The copper heat transfer element inside the hot heat exchanger (HHX) is of fin type with a fin thickness of 0.5 mm and a gap of 1 mm. The main ambient heat exchanger (MAHX) is of shell-tube type with working gas oscillating inside the stainless steel tubes with inner diameters of 2 mm and the chilling water flowing through the shell sides. The total number of the thin tubes is 301. The second ambient heat exchanger (2AHX) is also of the shell-tube type composed of 199 tubes with an inner diameter of 3 mm. In the experiments, the temperatures of the HHX and the AHXs are kept at 650 °C and 13 °C, respectively. The detailed dimensions of the traveling-wave thermoacoustic engine are listed in Table 1. Two

coupling positions are investigated in the experiments, as denoted by locations A and B in Figure 2. Location A is set near the connection between the compliance tube and the cone in the feedback loop, while location B is set near the left end of the gas resonator.

The schematic of the linear alternators, which are supplied by Lihan Thermoacoustic Technologies Co. Ltd, are depicted in Figure 3. The parameters of the linear alternators are given in Table 2. The two linear alternators are in a balanced opposed arrangement. The coils of the linear alternators are connected in series with an electric capacitance C_e and a variable load resistance R_l. The generated electric power is therefore dissipated by the load resistance.

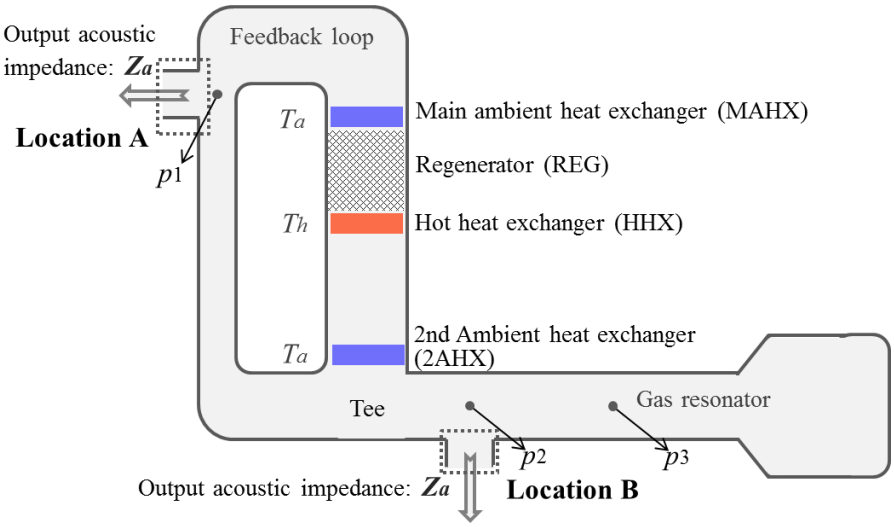


Figure 2. Two output locations of traveling-wave thermoacoustic engines

Table 1. Main geometric dimensions of traveling-wave thermoacoustic engine.

Component		Diameter/m	Length/m
AHX		0.09	0.056
REG		0.09	0.074
HHX		0.09	0.12
TBT		0.1	0.291
2AHX		0.1	0.02
Feedback loop (clockwise)	Tube near tee	0.09	0.295
	Cone	/	0.095
	Inertance tube	0.076	0.28
	Cone	/	0.1
	Compliance tube	0.1	0.6767
Resonator (left to right)	Tube near tee	0.09	0.095
	Cone	/	0.1
	Tube	0.1	2.3
	Cone	/	1.31
	Tube	0.261	0.52

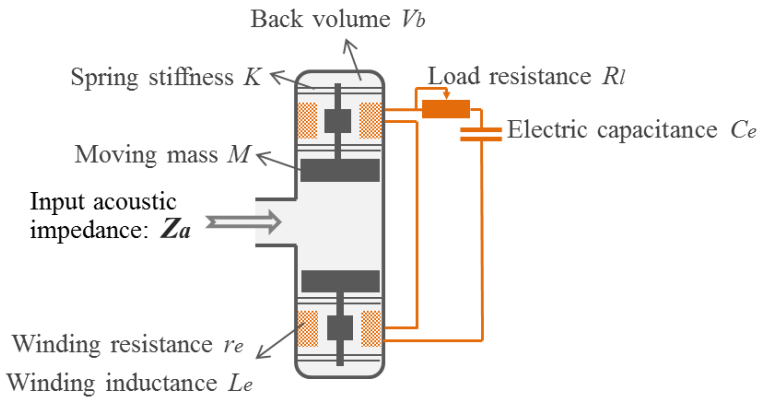


Figure 3. Schematic of linear alternators. The coils of the two linear alternators are connected in series with an electric capacitance C_e and a variable load resistance R_l.

Table 2. Parameters of linear alternators.

Parameters	#1	#2
Force factor Bl (N/A)	90	90
Winding inductance L_e (mH)	268	263.4
Winding resistance r_e (Ω)	3.58	3.56
Mechanical stiffness K (N/m)	189235	188844
Mechanical resistance R_m (Ns/m)	5	2
Moving mass M (kg)	1.097	1.079
Piston area A (cm^2)	19.635	19.635
Back volume V_b (L)	1.63	1.63

4. Output acoustic impedance of thermoacoustic engine

The thermoacoustic system is a distributed acoustic network system, which means the requirements of acoustic impedances for coupling the engine and the load are different at different output positions. Therefore, the output acoustic impedance characteristics can be simply modulated by changing the location for connecting the load.

A numerical model of the traveling-wave thermoacoustic engine is first built based on DeltaEC (Design Environment for Low-amplitude ThermoAcoustic Energy Conversion) [31]. Any acoustic load can be represented by an acoustic impedance with a real and imaginary part. In the numerical model, the built-in BRANCH component is used as the branched output acoustic impedance to couple with the engine at location A or B. The output acoustic power, thermoacoustic efficiency, pressure amplitude, volume flow rate, and frequency at different acoustic impedances can then be calculated by setting different values of the real and imaginary parts of the BRANCH component.

Then, the optimal ranges of the real and imaginary parts of the output acoustic impedances for the output performances of the thermoacoustic engine at different locations can be identified. In the calculations, the hot and ambient heat exchangers are set at 650 °C and 13 °C, respectively. Helium gas at 3.16 MPa is used as working fluid.

4.1 Operating frequency

Figure 4 shows the variation of operating frequency of the thermoacoustic engine with the output impedance at the two output locations. It is shown that the output acoustic impedance has weak effects on the operating frequency, especially at relatively high acoustic impedances. In general, the operating frequencies of the engine are around 65.5 Hz.

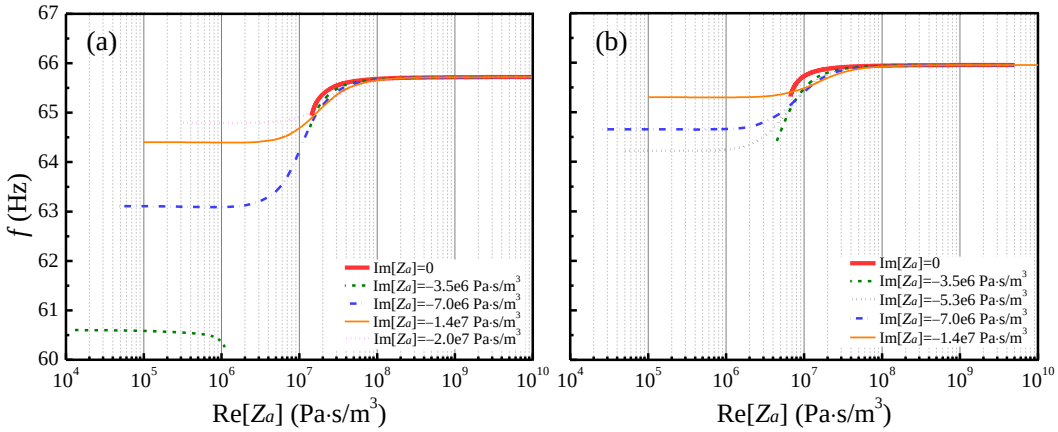


Figure 4. Operating frequency of traveling-wave thermoacoustic engine at (a) location A and (b) location B with respect to output acoustic impedance Z_a.

4.2 Output acoustic power and thermoacoustic efficiency

Figure 5 and Figure 6 shows the calculated output acoustic powers W_a and thermoacoustic efficiencies $\eta_{t\text{-}a}$ of the thermoacoustic engine at different output acoustic impedances Z_a when the acoustic load is coupled at locations A and B, respectively.

4.2.1 Location A

Variations of the output acoustic power and thermoacoustic efficiency of the thermoacoustic engine with the acoustic impedance at location A are given in Figure 5(a) and Figure 6(a), respectively. It is both beneficial for the power and the efficiency if the imaginary part Im[Z_a] of the output acoustic impedance approaches zero, which means the acoustic load is a pure acoustic resistance. Increasing the magnitude of Im[Z_a] results in a decrease of the maximum output acoustic power and the thermoacoustic efficiency, especially the latter one. When the imaginary part of the impedance is zero, the maximum output acoustic power and thermoacoustic efficiency are 795 W

and 0.292, respectively. The corresponding optimal real acoustic impedances Re[Z_a] are 3.8×10^7 Pa·s/m^3 and 1.8×10^7 Pa·s/m^3, respectively. The required output acoustic impedances of the engine for the maximum output acoustic power and thermoacoustic efficiency are not the same, and a compromise should be made when modulating the acoustic impedance of the load.

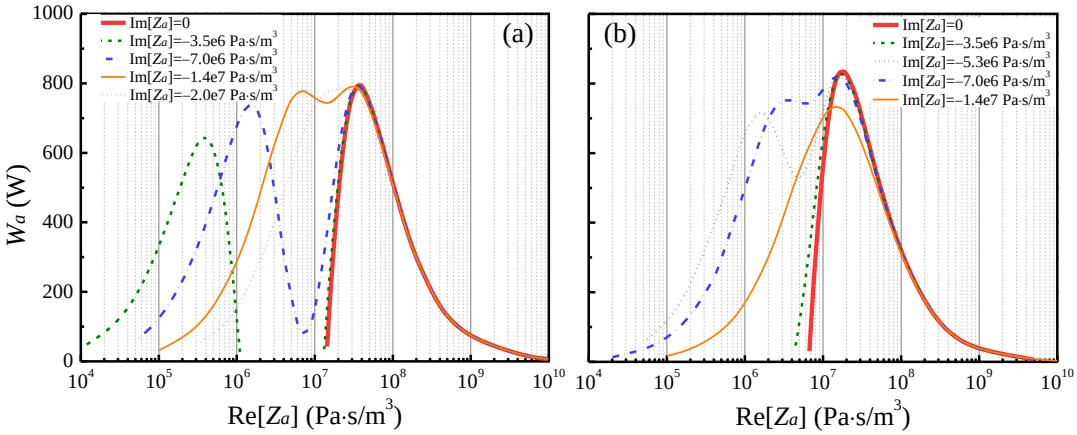


Figure 5. Output acoustic powers W_a of traveling-wave thermoacoustic engine at (a) location A and (b) location B with respect to output acoustic impedance Z_a.

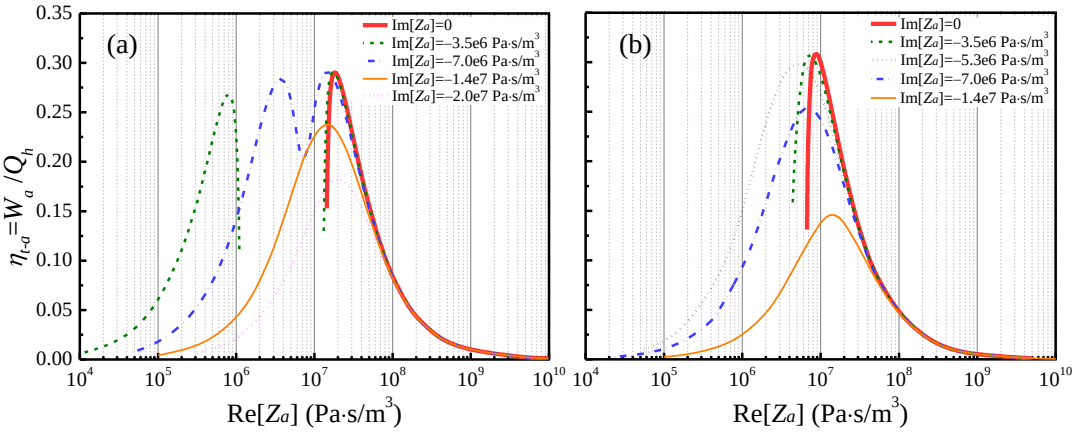


Figure 6. Thermoacoustic efficiencies $\eta_{t\text{-}a}$ of traveling-wave thermoacoustic engine at (a) location A and (b) location B with respect to output acoustic impedance Z_a.

4.2.2 Location B

Variations of the output acoustic power and thermoacoustic efficiency of thermoacoustic engine with the acoustic impedance at location B are given in Figure 5(b) and Figure 6(b), respectively. Similar to the trends with location A, both the output acoustic power and thermoacoustic efficiency are able to reach the higher maximum values when the imaginary part of the output acoustic impedance approaches zero. Compared with the output performance at location A, both the maximum output acoustic power and thermoacoustic efficiency at location B are both a little higher, and the required real acoustic impedances are much smaller. When the imaginary output acoustic impedance Im[Z_a] is zero, the maximum output acoustic power of 837 W and highest

thermoacoustic efficiency of 0.31 are achieved at the real output acoustic impedances Re[Z_a] of 1.8×10^7 Pa·s/m^3 and 9×10^6 Pa·s/m^3, respectively.

When Im[Z_a] is set at -3.5×10^6 Pa·s/m^3, the maximum output acoustic power and thermoacoustic efficiency both have tiny decreases compared with those at zero Im[Z_a]. However, the ranges to achieve the relatively high acoustic power and efficiency are enlarged, which makes it easier for adjusting the acoustic impedance of the linear alternator to fall into the sweet spot range. When Im[Z_a] is far away from zero, for example at the scale of 10^7 Pa·s/m^3, the performances of the thermoacoustic engine are largely degraded. The thermoacoustic efficiency is more sensitive to the imaginary output acoustic impedance than the output power.

4.3 Equivalent displacement

During the modulation of the acoustic impedance, the output acoustic power may exceed the maximum value that can be extracted by the linear alternators, and make the linear alternator be overloaded in displacements. Therefore, it is necessary to investigate the volume flow rate required to couple with the engine at different acoustic impedances. The volume flow rate $|U_1|$ at the output position is converted into the equivalent displacement $|x_1|$ of the linear alternators by using the relationship of $|x_1|=0.5|U_1|/\omega A$. The equivalent displacement can be used to check whether the displacement of the linear alternators is within the safe range of 6.5 mm at certain acoustic impedances.

Figure 7 shows the calculated equivalent displacements at the two output positions. Similar to the relations of the distributions of the output acoustic power and thermoacoustic efficiency, the corresponding real acoustic impedances for the maximum equivalent displacements at imaginary acoustic impedances close to zero are a little larger at the location A. Due to the much larger magnitude of the acoustic impedances at location A, the equivalent displacements at location A are generally smaller than those at location B when Re[Z_a] is above 10^7 Pa·s/m^3. When Im[Z_a] is smaller than -1.4×10^7 Pa·s/m^3 at location A and -5.3×10^6 Pa·s/m^3 at location B, the equivalent displacements increases dramatically to values that are much larger than 6.5 mm when decreasing Re[Z_a] from 10^7 Pa·s/m^3. Recalling the output performances given in Figure 5 and 6, though relatively good performances can still be obtained at these impedances, it is not appropriate to couple the linear alternators with the engine at these acoustic impedance ranges due to the overloaded displacements. When Re[Z_a] is higher than 10^7 Pa·s/m^3, the equivalent displacements are mainly within the safe range.

For location A, the corresponding equivalent displacements for the maximum output acoustic power and thermoacoustic efficiency are only about 4 mm. For location B, they are 5.93 mm and 6.17 mm respectively, which are also within the safe range. It means that it is feasible for the linear alternators to couple with the engine at these optimal acoustic impedances.

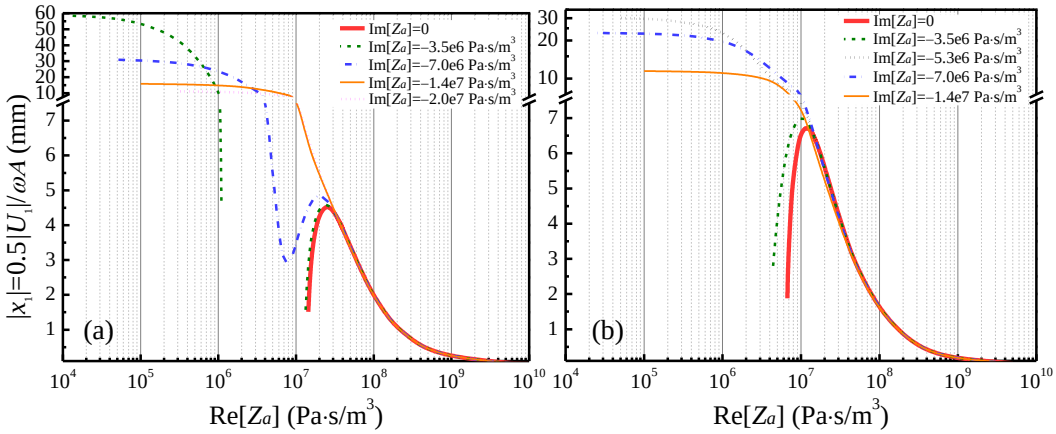


Figure 7. Equivalent displacements $|x_1|$ at (a) location A and (b) location B with respect to output acoustic impedance Z_a.

5. Input acoustic impedance of linear alternators

The acoustic impedance of one linear alternator is expressed as [14, 16],

$$Z_a = \frac{1}{A^2}\left[\left(R_m + \frac{R_e Bl^2}{R_e^2 + X_e^2}\right) + j\left(X_m - \frac{X_e Bl^2}{R_e^2 + X_e^2}\right)\right] \tag{2}$$

where $X_e = \omega M - K/\omega$, $R_e = R_l + r_e$, and $X_e = \omega L_e - 1/\omega C_e$. According to the above equation, the input acoustic impedance of the linear alternators can be modulated by adjusting the operating frequency f, load resistance R_l, and electric capacitance C_e for specific linear alternators.

5.1 Effect of operating frequency

Figure 8 shows the dependences of input acoustic power and output electric power on operating frequency for one linear alternator at fixed pressure amplitude and load resistance. As shown, when the operating frequency is about 71 Hz, which is near the resonant frequency of the linear alternator, both the input acoustic power and the output electric power reach their maximums.

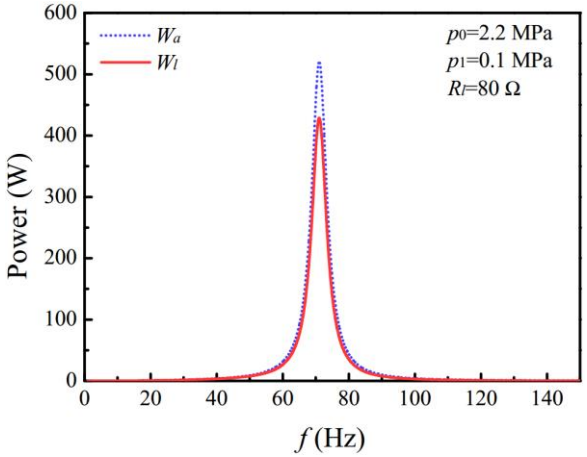


Figure 8. Input acoustic power and output electric power vs. operating frequency.

The variations of the acoustic impedances of the linear alternator with the operating frequency are shown in Figure 9. When the operating frequency increases from 10 Hz to 150 Hz, the imaginary part of the input acoustic impedance of the linear alternator increases from a minus value to a positive one, while the real part decreases remarkably from 3×10^7 Pa·s/m^3 to only 4.7×10^6 Pa·s/m^3. The imaginary part of the acoustic impedance reaches zero at the resonant frequency. According to the electroacoustic analogy, the equivalent acoustic power factor of the linear alternator at the fixed driven pressure amplitude reaches one when it is at resonant frequency. This is why the acoustic power extracted and the electric power generated at the resonant frequency reach the maximums.

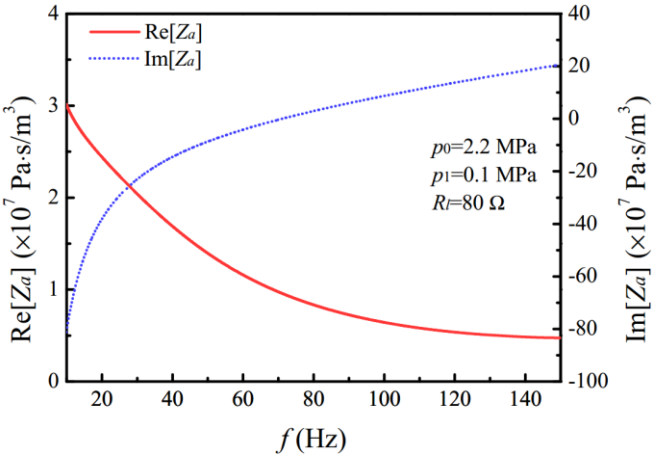


Figure 9. Input acoustic impedances vs. operating frequency.

In all, the above analysis shows that the ability to extract the acoustic power of the linear alternators is the strongest at the resonant frequency. When the operating frequency is far away from the resonant one, the acoustic power that can be extracted by the linear alternator is largely decreased due to the large acoustic reactance.

5.2 Effect of electric capacitance

Figure 10 and Figure 11 shows the effects of the connected electric capacitance on the input acoustic impedance and acoustoelectric efficiency of the two linear alternators when the load resistance is at 100 Ω and 180 Ω, respectively.

According to Figure 10, the real and imaginary parts of the acoustic impedance both approach constant values at very large or small electric capacitances. When the electric capacitance is very small, i.e. less than 1 μF, the imaginary and real parts approach -5.4×10^6 Pa·s/m^3 and 5.2×10^5 Pa·s/m^3, respectively. According to the output characteristics of the thermoacoustic engine, as illustrated in Figure 5 and Figure 6, the above acoustic impedance is far away from the optimal ranges for both the location A and location B. What is more, the acoustoelectric efficiency at the small electric capacitance is also very limited, as shown in Figure 11. Similarly, when the electric capacitance is larger than 100 μF, the real and the imaginary parts of the acoustic impedance approach around 5×10^6 Pa·s/m^3 and -1.3×10^7 Pa·s/m^3, respectively. The corresponding equivalent

displacements of the linear alternator will reach more than 11 mm at location A and 9 mm when connecting at location B, which are much larger than the maximum allowable value of 6.5 mm. The above analysis shows that the linear alternators cannot be matched to the thermoacoustic engine at either location A or location B when the electric capacitance is either larger than 100 μF or smaller than 1 μF.

Fortunately, when the circuit is connected with an electric capacitance of about 10 μF, both the real and the imaginary parts of the acoustic impedance can be effectively modulated to meet the requirements for matching with the thermoacoustic engine. According to Figure 10, when the electric capacitance is adjusted to be around 10 μF, the imaginary part of the acoustic impedance is very close to zero, and the real part can be adjusted from 1.16×10^7 Pa·s/m^3 to 1.92×10^7 Pa·s/m^3 by increasing the load resistance from 100 Ω to 180 Ω. According to the output characteristics of the engine at location A, the acoustic impedances of the linear alternators partly cover the required range for optimal performances. For the location B, the above range of the acoustic impedances of the linear alternators meets the requirements for achieving the maximum output power of the thermoacoustic engine. The optimal operation point for thermoacoustic efficiency of the engine at the location B can be reached by using a larger load resistance or an electric capacitance a little

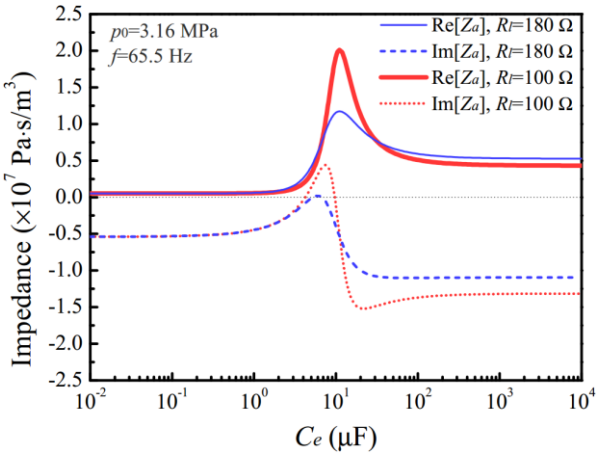


Figure 10. Effect of electric capacitance on input acoustic impedance of linear alternators.

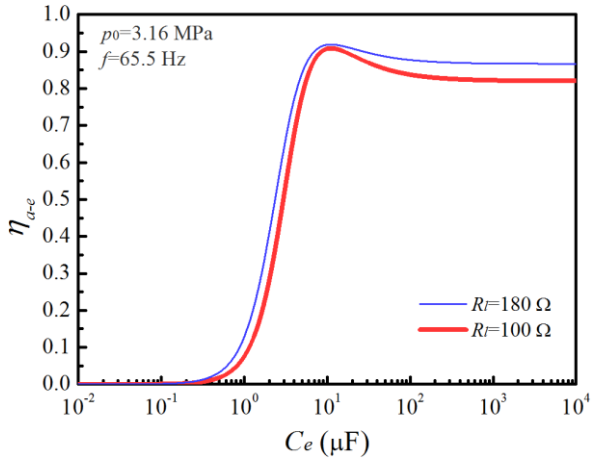


Figure 11. Effect of electric capacitance on acoustoelectric efficiency of linear alternators.

smaller than 10 μF. Moreover, the acoustoelectric efficiency of linear alternators also reaches its maximums when the electric capacitance is 10 μF, as shown in Figure 11. In all, both the thermoacoustic engine and the linear alternators work at their optimal working conditions when they are coupled at location B and the electric capacitance is around 10 μF. It denotes that the system is acoustically matched and the optimal performance can be obtained at the location B.

5.3 Effect of load resistance

Figure 12 and Figure 13 show the effects of the load resistance on the input acoustic impedance and acoustoelectric efficiency of the linear alternators when the electric capacitance is 9.6 μF, which is consistent with that used in the following experiments. As shown in Figure 12, when no electric capacitance is connected in the circuit, both the real and imaginary parts of the acoustic impedance have very limited variation ranges when adjusting the load resistance. Whereas, if the electric capacitance of 9.6 μF is connected, the acoustic impedances can be easily modulated in a large range, especially when the load resistance is below 200 Ω. It indicates that the load resistance has great effects on the real and imaginary parts of the input acoustic impedance of the linear alternator, which makes it possible to modulate the acoustic impedance in a large enough range to match with the thermoacoustic engine. The imaginary part of the acoustic impedance decreases rapidly from a positive value to a negative one when increasing the load resistance, and reaches about zero at 100 Ω. The corresponding real part of the acoustic impedance is 1.83×10^7 Pa·s/m^3, which is very close to the optimal point for output acoustic power of the engine at location B.

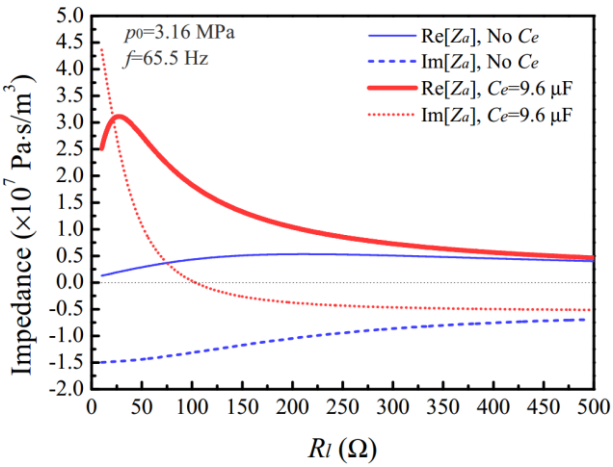


Figure 12. Effect of load resistance on input acoustic impedance of linear alternators.

As shown in Figure 13, the acoustoelectric efficiency of the linear alternators first increases and then has a slightly decrease when increasing the load resistance. The efficiency with the electric capacitance is higher than that without an electric capacitance at any load resistance, showing the importance of the electric capacitance. When the electric capacitance of 9.6 μF is adopted, the acoustoelectric efficiency is all the way above 0.9 when the load resistance is within the range of 80 Ω~340 Ω.

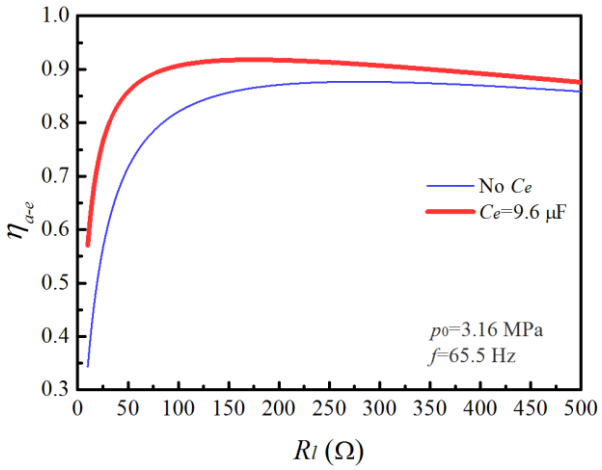


Figure 13. Effect of load resistance on acoustoelectric efficiency of linear alternators.

6. Acoustic impedance matching of the system

In this section, the thermoacoustic engine and the linear alternators are coupled to form a combined system to study the characteristics of the impedance match numerically and experimentally.

6.1 Matching of operating frequency

The operating frequency is adjusted by using two different working gas, i.e. helium and nitrogen gases in the experiments. The experiments for investigating the effect of operating frequency on the overall performances are conducted by using one linear alternator #2 connected at the location B of the thermoacoustic engine. The filling pressure is 2.2 MPa.

When nitrogen is used as working fluid, the operating frequency of the whole system is about 23 Hz, which is much lower than the mechanical resonant frequency of the linear alternator. When helium gas is used, the operating frequency reaches 65 Hz, which is very close to the resonant frequency. Figure 14 shows the electric powers W_l and thermal-to-electric efficiencies $\eta_{t\text{-}e}$ of the electric generator system with the above working fluids. It shows that both the electric power and the efficiency of the system with helium as the working fluid are much higher than those with nitrogen. For example, when the load resistance is 80 Ω, the system with helium achieves an electric power of 107 W and an efficiency of 0.0325, while that with nitrogen only has 4.1 W and 0.0016, respectively. The optimal output acoustic power of the engine with nitrogen is about 260 W. Though the output performance with nitrogen is intrinsically smaller than that with helium, the large difference between the obtained electric power and the optimal output acoustic power indicates that the impedance is far away from the optimal one when nitrogen is used due to the mismatch of the frequencies. The results show that the match of the operating frequency is critical to the impedance match of the thermoacoustic electric generator.

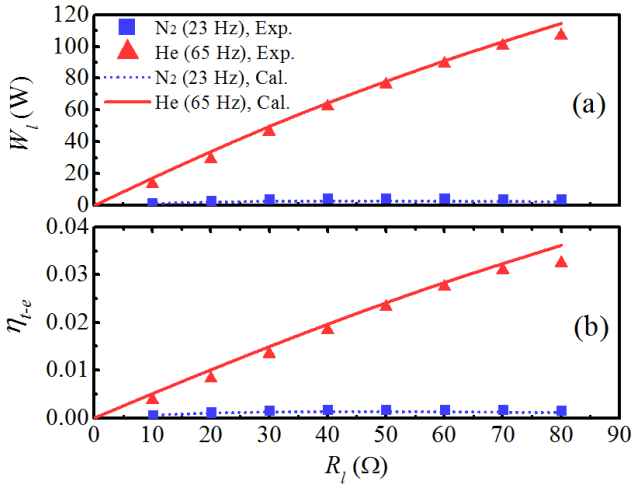


Figure 14. Comparisons of electric power and thermal-to-electric efficiency with helium and nitrogen gas as working fluid.

6.2 Coupled at location A

Based on the above analysis about the match of the operating frequency, helium is used as the working fluid in the following experiments. The filling pressure is 3.16 MPa. Two linear alternators are first coupled with the thermoacoustic engine at location A. According to the acoustic impedance characteristics of the linear alternators, the required impedances for coupling the engine at location A are predicted to be partly covered by adding an electric capacitance of 9.6 μF and adjusting the load resistance to be relatively small. Experiments and numerical simulations are then conducted on the thermoacoustic electric generator with an electric capacitance of 9.6 μF connected in the circuit.

Figure 15 and Figure 16 shows the frequency, pressure amplitude, displacement, and electric current of the thermoacoustic electric generator when the engine and the alternator are coupled at location A. All the four calculated parameters have good agreements with the experimental ones, showing the good accuracy of the numerical model.

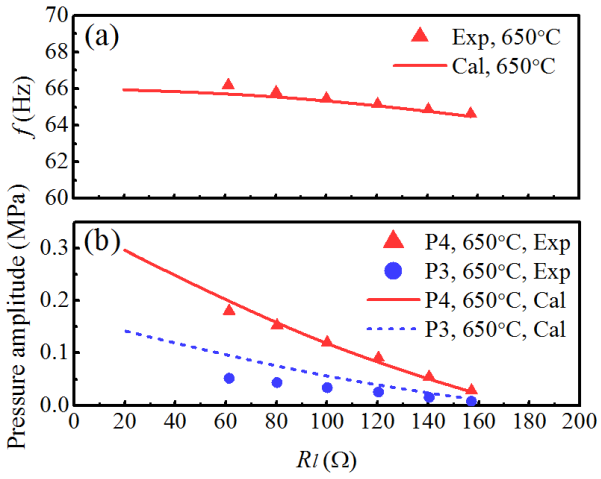


Figure 15. Operating frequency and pressure amplitude when linear alternators are connected at location A.

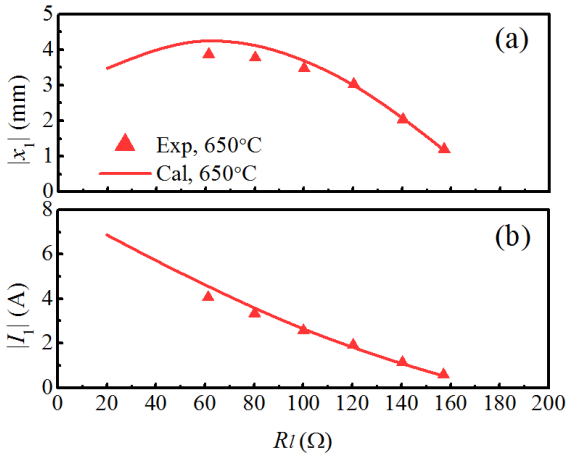


Figure 16. Displacement and electric current when linear alternators are connected at location A.

The output performances of the system when the engine and the alternators are coupled at location A are shown in Figure 17. When decreasing the load resistance from 160 Ω to 60 Ω, the output electric power increases remarkably due to the increase of the real acoustic impedance, which is approaching the optimal one. The maximum electric power reaches 506.4 W in the experiments. Tests are not conducted below 60 Ω for the safety concerns. The highest thermal-to-electric efficiency reaches 0.146. The difference between experimental and calculated results may result from the underestimated losses in the model, including the losses from the membrane, the heat transfer losses and the nonlinear losses at high amplitudes.

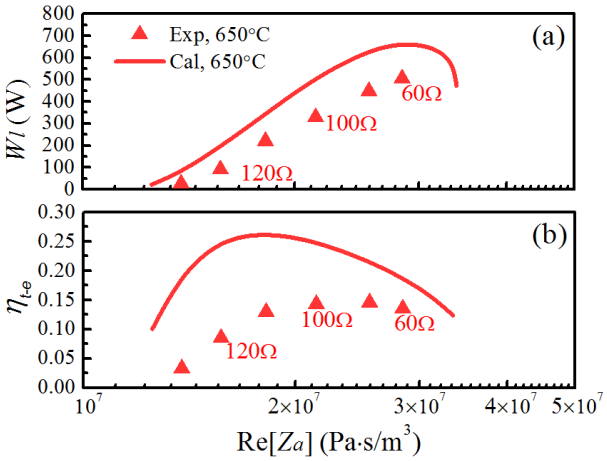


Figure 17. Output electric power and thermal-to-electric efficiency when linear alternators are connected at location A.

6.3 Coupled at location B

According to the output acoustic impedance of the thermoacoustic engine and the input acoustic impedance of the linear alternators, the engine and the alternators can be better matched at

location B by adjusting the electric capacitance and the load resistance to be 9.6 μF and 100 Ω, respectively.

Figure 18 shows the operating frequency and pressure amplitudes of the system when the two linear alternators are connected at location B with heating temperatures of 650 °C and 600 °C. The numerical and experimental results agree very well in both tendency and magnitude. The small differences may result from some small geometric differences between the calculations and the experiments. The temperatures of the tube walls increase to higher values than the ambient temperature due to the acoustic power dissipations and thermal conductions. This may also generate deviations between the calculations and the experiments. Figure 19 shows the displacements of the linear alternator #2 and the electric current. The simulations are also in good agreements with the experiments. The displacement increases while the electric current decreases with the load resistance. Therefore, there are upper and lower bounds for the load resistance. It is adjusted in the ranges of 100 Ω~180 Ω and 100 Ω~240 Ω when the heating temperature is 650 °C and 600 °C, respectively.

The displacements at locations A and B have reverse tendencies. The differences essentially result from the different distributions of the equivalent displacements with the real acoustic impedances. When the system is coupled at location B, the variation range of the real acoustic impedance is between 1×10^7 Pa·s/m^3 and 2×10^7 Pa·s/m^3, which is at the right side of the corresponding acoustic impedance for the maximum displacement, according to the equivalent displacement diagram given in Figure 7(b). Therefore, the displacement increases when increasing the load resistance due to the reduced real acoustic impedance. However, when it is at location A, the variation range of the real acoustic impedance is within 1×10^7~3×10^7 Pa·s/m^3. According to Figure 7(a), it is at the left side of the corresponding impedance for the maximum displacement, resulting in the distribution of the displacement shown in Figure 16.

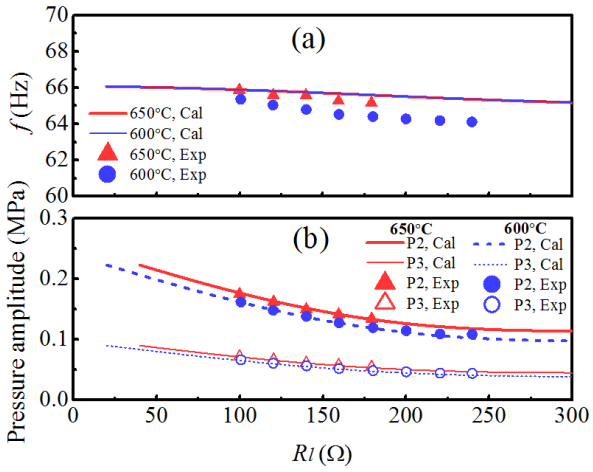


Figure 18. Operating frequency and pressure amplitude when linear alternators are connected at location B.

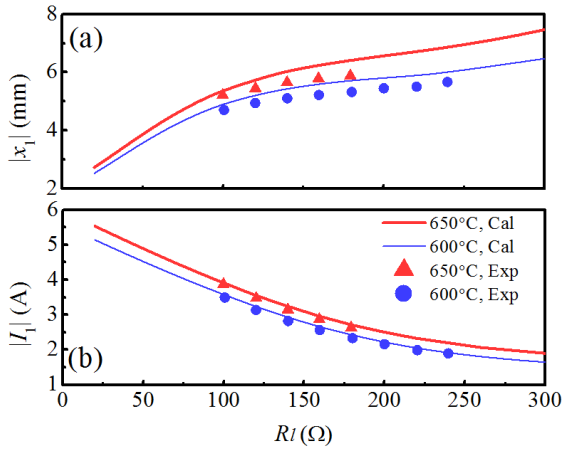


Figure 19. Displacement and electric current when linear alternators are connected at location B.

Figure 20 shows the relationship of output electric power of the coupled system with the real part of the acoustic impedance of the linear alternators. When the heating temperature is fixed at 650 °C, the electric power reaches its maximums of 765.8 W in the simulations and 750.4 W in the experiments at 100 Ω, which is much larger than that coupled at location A. The acoustic impedance at 100 Ω indicates that it is at the optimal point for the output electric power of the coupled system, as well as the optimal one for the output acoustic power of the engine. The output electric power decreases when increasing the load resistance from 100 Ω to 180 Ω due to the shrinking of the output acoustic power which results from the reduction of the real part of the acoustic impedance. Similar trend of the output electric power is observed at 600 °C. The maximum electric power reaches 614.9 W in the experiments at 100 Ω. The calculated electric powers show good agreements with the experimental ones at both heating temperatures.

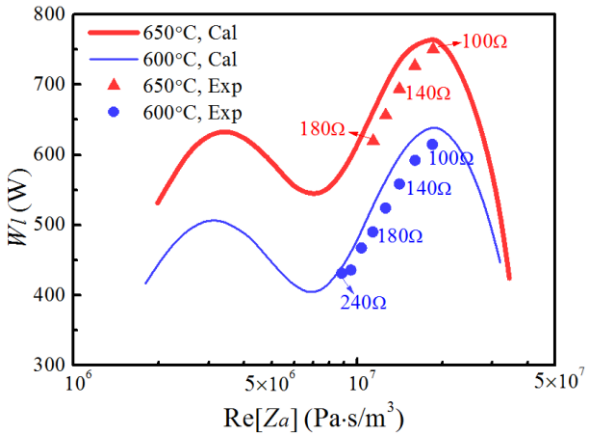


Figure 20. Output electric power when linear alternators are connected at location B.

Figure 21 shows the thermal-to-electric efficiency of the thermoacoustic electric generator at different heating temperatures. The highest efficiencies are reached at relatively higher load resistances, which is different from the acoustic powers. This is because that the optimal range of the real part of acoustic impedance for the thermoacoustic efficiency of the thermoacoustic engine

is smaller than that for the acoustic power. The thermoacoustic electric generator reaches the highest thermal-to-electric efficiency of 0.163 at 160 Ω when the heating temperature is fixed at 650 °C in the experiments, which is also higher than that at location A. The trends of the numerical results are similar to the experimental ones. The deviations between the experimental and the numerical results mainly result from the underestimated heat losses from the HHX in the modeling, including the heat radiation and convection to the surroundings and the 2AHX through the TBT, and the heat conduction through the pipes and the REG. Besides, backup heating elements in the periphery of the HHX which have a much worse heat transfer performance are used to supply the required heating power.

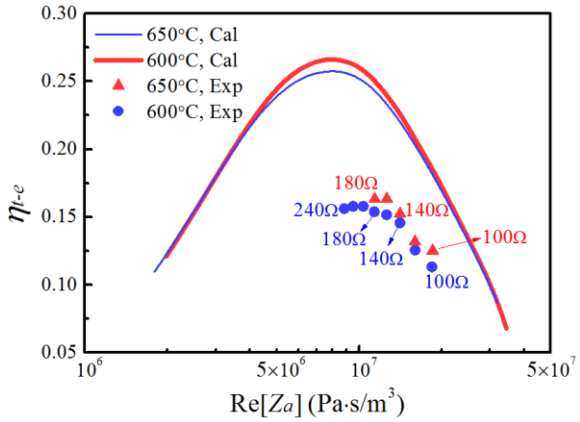


Figure 21. Thermal-to-electric efficiency when linear alternators are connected at location A.

7. Conclusions

The impedance match of a thermoacoustic electric generator which is composed of a traveling-wave thermoacoustic engine and a pair of linear alternators is studied. The general procedure for the impedance match is proposed systematically. The optimal acoustic impedances for the best performances of the thermoacoustic engine are then identified numerically by analyzing the output acoustic impedance characteristics. Two different coupling positions, including location A at the feedback loop and location B at the resonator, are investigated to modulate the output acoustic impedances of the engine. It is found that it is beneficial for the output performances of the engine at both locations when the imaginary parts of the output acoustic impedance of the engine is close to zero. The optimal real part of the output acoustic impedances at location A is relatively higher than that at location B due to the larger local acoustic impedances. Numerical analyses of the acoustic characteristics of the linear alternators indicate that the acoustic impedance of the linear alternators can be modulated to cover the optimal range required by the thermoacoustic engine at location B and partly cover the required one at location A by adjusting the operating frequency to be near the resonant frequency and the electric capacitance to be near 10 μF.

The thermoacoustic engine and the linear alternators are finally coupled at location A and location B, respectively. The comparisons of the output performances of the system at different

coupling locations indicate that the coupling location has a great effect on the impedance match of the system. The system achieves the maximum output electric power of 750.4 W and the highest thermal-to-electric efficiency of 0.163 at location B. Both the simulations and the experiments show that the thermoacoustic engine and the linear alternators are acoustically well matched at location B.

Acknowledgements

This work was supported by National Natural Science Foundation of China under contract No. 51476136 and China Postdoctoral Science Foundation under contract No. 2013M541772.

References

[1] M.E.H. Tijani, S. Spoelstra, A hot air driven thermoacoustic-Stirling engine, Applied Thermal Engineering, 61 (2013) 866-870.

[2] Y.W. Liu, P. Yang, Influence of inner diameter and position of phase adjuster on the performance of the thermo-acoustic Stirling engine, Applied Thermal Engineering, 73 (2014) 1141-1150.

[3] S. Hasegawa, T. Yamaguchi, Y. Oshinoya, A thermoacoustic refrigerator driven by a low temperature-differential, high-efficiency multistage thermoacoustic engine, Applied Thermal Engineering, 58 (2013) 394-399.

[4] D.M. Sun, L.M. Qiu, B. Wang, Y. Xiao, Novel Helmholtz resonator used to focus acoustic energy of thermoacoustic engine, Applied Thermal Engineering, 29 (2009) 945-949.

[5] D.M. Sun, L.M. Qiu, B. Wang, Y. Xiao, L. Zhao, Output characteristics of Stirling thermoacoustic engine, Energy Conversion and Management, 49 (2008) 1265-1270.

[6] K. Wang, D.M. Sun, J. Zhang, J. Zou, K. Wu, L.M. Qiu, Z.Y. Huang, Numerical simulation on onset characteristics of traveling-wave thermoacoustic engines based on a time-domain network model, International Journal of Thermal Sciences, 94 (2015) 61-71.

[7] K. Wang, D.M. Sun, J. Zhang, N. Zhang, K. Luo, L.M. Qiu, Beating effect between a thermoacoustic source and its mechanical partner, Journal of Applied Physics, 118 (2015) 244907.

[8] X.Q. Zhang, J.Z. Chang, Onset and steady-operation features of low temperature differential multi-stage travelling wave thermoacoustic engines for low grade energy utilization, Energy Conversion and Management, 105 (2015) 810-816.

[9] T.J. Bi, Z.H. Wu, L.M. Zhang, G.Y. Yu, E.C. Luo, W. Dai, Development of a 5 kW traveling-wave thermoacoustic electric generator, Applied Energy, (2015) (In Press).

[10] S. Backhaus, E. Tward, M. Petach, Traveling-wave thermoacoustic electric generator, Applied Physics Letters, 85 (2004) 1085-1087.

[11] S.M. Oriti, N.A. Schifer, Recent Stirling Conversion Technology Developments and Operational Measurements at NASA Glenn Research Center, in: 7th International Energy Conversion and Engineering Conference (IECEC 2009), Denver, CO, USA, 2009.

[12] Y.F. Wang, Z.Y. Li, Q. Li, A novel method for improving the performance of thermoacoustic electric generator without resonator, Energy Conversion and Management, 110 (2016) 135-141.

[13] Z.H. Wu, W. Dai, M. Man, E.C. Luo, A solar-powered traveling-wave thermoacoustic electricity generator, Solar

Energy, 86 (2012) 2376-2382.
[14] Z.H. Wu, L.M. Zhang, W. Dai, E.C. Luo, Investigation on a 1 kW traveling-wave thermoacoustic electrical generator, Applied Energy, 124 (2014) 140-147.
[15] Z.H. Wu, G.Y. Yu, L.M. Zhang, W. Dai, E.C. Luo, Development of a 3 kW double-acting thermoacoustic Stirling electric generator, Applied Energy, 136 (2014) 866-872.
[16] D.M. Sun, K. Wang, X.J. Zhang, Y.N. Guo, Y. Xu, L.M. Qiu, A traveling-wave thermoacoustic electric generator with a variable electric R-C load, Applied Energy, 106 (2013) 377-382.
[17] K. Wang, D.M. Sun, J. Zhang, Y. Xu, J. Zou, K. Wu, L.M. Qiu, Z.Y. Huang, Operating characteristics and performance improvements of a 500 W traveling-wave thermoacoustic electric generator, Applied Energy, 160 (2015) 853-862.
[18] Z.B. Yu, A.J. Jaworski, S. Backhaus, A low-cost electricity generator for rural areas using a travelling-wave looped-tube thermoacoustic engine, Proceedings of the Institution of Mechanical Engineers, Part A: Journal of Power and Energy, 224 (2010) 787-795.
[19] Z.B. Yu, A.J. Jaworski, S. Backhaus, Travelling-wave thermoacoustic electricity generator using an ultra-compliant alternator for utilization of low-grade thermal energy, Applied Energy, 99 (2012) 135-145.
[20] H.F. Kang, P. Cheng, Z.B. Yu, H.F. Zheng, A two-stage traveling-wave thermoacoustic electric generator with loudspeakers as alternators, Applied Energy, 137 (2015) 9-17.
[21] K. de Blok, On the design of near atmospheric air operated thermoacoustic engines, in: Aster (ed.), 2013. [http://www.aster-thermoacoustics.com/wp-content/uploads/2013/09/Design-and-build-of-a-50W-thermacoustic-generator2.pdf].
[22] G.W. Swift, Thermoacoustic engines, The Journal of the Acoustical Society of America, 84 (1988) 1145-1180.
[23] R.S. Wakeland, Use of electrodynamic drivers in thermoacoustic refrigerators, The Journal of the Acoustical Society of America, 107 (2000) 827-832.
[24] M.E.H. Tijani, Loudspeaker-driven thermo-acoustic refrigeration, in, Vol. Ph.D. Dissertation, Eindhoven University of Technology, Eindhoven, 2001.
[25] C. Jensen, R. Raspet, Thermoacoustic power conversion using a piezoelectric transducer, The Journal of the Acoustical Society of America, 128 (2010) 98-103.
[26] L. Fan, S.Y. Zhang, B.R. Wang, Coupling between thermoacoustic resonance pipes and piezoelectric loudspeakers studied by equivalent circuit method, Journal of the Acoustical Society of America, 120 (2006) 1381-1387.
[27] D. Marx, X. Mao, A.J. Jaworski, Acoustic coupling between the loudspeaker and the resonator in a standing-wave thermoacoustic device, Applied Acoustics, 67 (2006) 402-419.
[28] W. Dai, E.C. Luo, X.T. Wang, Z.H. Wu, Impedance match for Stirling type cryocoolers, Cryogenics, 51 (2011) 168-172.
[29] H. Hatori, T. Biwa, T. Yazaki, How to build a loaded thermoacoustic engine, Journal of Applied Physics, 111 (2012) 074905.
[30] L.M. Zhang, Y.Y. Chen, E.C. Luo, How to match an acoustical load to a thermoacoustic heat engine?, AIP Conference Proceedings, 1573 (2014) 1445-1452.
[31] B. Ward, J. Clark, G.W. Swift, Design Environment for Low-amplitude Thermoacoustic Energy Conversion. Version 6.2. Users Guide., 2008.